Kent Academic Repository

Full text document (pdf)

Study on optimization of nano-coatings for ultra-sensitive biosensors based on long-period fiber grating

Sankhyabrata Bandyopadhyay[a], Liyang Shao[a,*], Chao Wang[a,b], Shuaiqi Liu[a], Qiang Wu[c], Guoqiang Gu[a], Jie Hu[a], Yanjun Liu[a], Xiaolong Chen[a], Zhangqi Song[a], Xuefeng Song[a], Qiaoliang Bao[d], Mateusz Smietana[e]

[a] *Department of Electrical and Electronic Engineering, Southern University of Science and Technology, Shenzhen 518055, Guangdong, China*

[b] *School of Engineering and Digital Arts, University of Kent, Canterbury CT27NT, United Kingdom*

[c] *Faculty of Engineering and Environment, Northumbria University, Newcastle Upon Tyne NE1 8ST, United Kingdom*

[d] *Department of Materials Science and Engineering, ARC Centre of Excellence in Future Low-Energy Electronics Technologies (FLEET), Monash University, Clayton, Victoria 3800, Australia*

[e] *Warsaw University of Technology, Institute of Microelectronics and Optoelectronics, Koszykowa 75, 00–662 Warszawa, Poland*

ARTICLE INFO

ABSTRACT

Bio-chemical sensors are expected to offer high sensitivity and specificity towards the detection of an analyte. It has been found that optical sensors based on long period fiber gratings (LPFGs) meet most of these requirements, particularly when coated with thin and high-refractive index overlays with proper bio-functionalization. In this paper, the influence of properties of the overlay material on the sensitivity of LPFG sensors to bio-analytes is analyzed. It has been observed that the sensitivity of a particular cladding mode of LPFG can be changed drastically with the adhesion of few tens of 'nm' of bio-layers to the surface of LPFG. "Volume refractive index sensitivity" and "add-layer sensitivity" of a particular cladding mode, dynamic range, and limit of detection of the sensors have been investigated in the context of overlay materials, bio-functionalization steps, and surrounding buffer medium. The selection criteria of the thin-film deposition technique are discussed with the aim of designing highly sensitive sensors for biological and chemical applications. Concept of optimum overlay thickness has been redefined and an effective case-specific design methodology is proposed.

1. Introduction

High sensitivity, fast response time, reliability and capability for label-free in situ measurements of specific analyte make optical fiber sensors a suitable component for distinct chemical and biological sensing applications. They are certainly among the most attractive research fields over the past few decades [1,2]. Modulation of optical properties of core/cladding modes with change in surrounding refractive index (SRI) is the backbone principle of this family of sensors. Optical fiber grating-based sensors have established itself as a promising platform of label-free optical biosensors and chemical sensors over the last decade or so [3–9]. A long-period fiber grating (LPFG), which is a periodic modulation of the refractive index (RI) in the core of an optical fiber, is of particular interest. The period of this grating structures reaches a few hundreds of micrometers, and is much longer than that of a fiber Bragg grating (FBG), has attracted great interest in sensing applications as the long periodic modulation of RI initiates coupling of light between the

forward propagating core mode and forward propagating cladding modes, and as a result, a series of resonance bands can be found in the transmission spectrum of the LPFG. These cladding modes are more sensitive to SRI changes [10,11]. Wavelength of the resonance band of a particular cladding mode depends on the effective index of core mode, effective index of cladding mode and the period of that grating. The effective index of cladding mode changes with the alteration in SRI and as a result, a shift in resonance band of cladding mode can be observed in the output spectrum. This is the basic principle of LPFG based RI sensors. LPFGs are being used for the measurement of the change in SRI successfully over the past decade [11]. The measurement of the change of SRI near the water medium is of the utmost importance as most of the chemical/biochemical sensors are designed to work in water or water-like buffer media. With the advancement of the research over the years, LPFG has now become a very attractive platform for specific bio-chemical sensing applications [3]. Numerous methods have been proposed over the past few years for enhancement of the sensitivity of LPFG
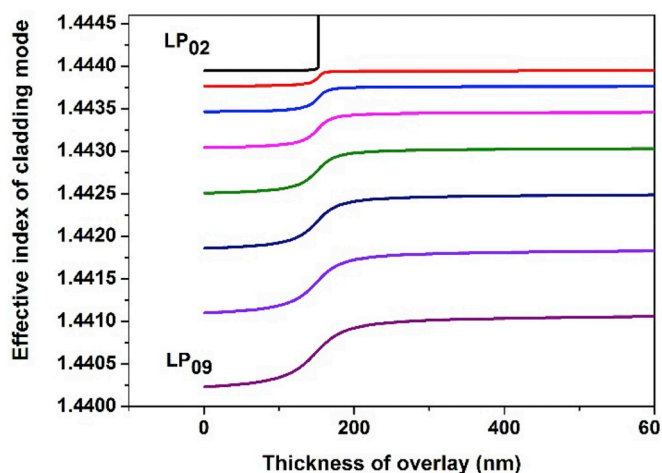
Fig. 1. Effect of MT phenomenon on effective refractive index of cladding modes with deposition of overlay. The RI of the overlay was assumed to be 1.7. standard parameters of single mode fiber is used for the simulation.

sensors in SRI sensing [12–16]. In particular, the mode transition (MT) effect of cladding modes was used extensively for this purpose [13–15]. To enable a significant MT effect, a thin layer, which has an RI higher than cladding material and a thickness of several hundred nanometers, was deposited over the fiber surface [13–15,17]. With an increase of the thickness of overlay, effective index of the cladding modes organizes in such a way that beyond a certain overlay thickness the lowest order cladding mode starts to be guided by the overlay and rest of the higher-order cladding modes experience transition to their preceding lower-order cladding mode as it is shown in Fig. 1 [12]. Different deposition techniques have already been used successfully over the past decade for the deposition of an overlay. Liquid precursors-based techniques such as Langmuir-Blodgett [18], electrostatic self-assembly [13,19], or dip coating [6,15,20] have been used tandemly for the deposition of overlay. Chemical vapor deposition [17,21], thermal evaporation [22], sputtering [23], crystal growth technique [24] and atomic layer deposition [25] are mostly vapor-based techniques used for deposition of overlay. Sensitivity defined for certain resonance corresponding to a cladding mode of LPFG depends on RI of overlay material, its thickness, and SRI. The sensitivity near RI of water (~1.333RIU) varies from ~1500 nm/refractive index unit (RIU) for deposition of a polymeric material (RI ~ 1.5 RIU) up to near ~10,000 nm/RIU when RI of the overlay exceeding 2 for specific metal oxide layers [6,13,25]. An alternative method to enhance the sensitivity to operate cladding mode of LPFG near the turn-around point (TAP) [12] or dispersion turning point (DTP) [29]. It was reported that with tuning the initial coupling conditions near the TAP of a particular cladding mode the sensitivity can be enhanced significantly [16]. The enhancement of the sensitivity of LPFG in SRI sensing with the deposition of gold nanoparticles at TAP was demonstrated recently [26]. The sensitivity can be enhanced even more when combining the effect of MT and TAP of a particular cladding mode. A theoretical study showed that sensitivity can reach as high as 100,000 nm/RIU when these two techniques are combined [14]. Later experimental validation of this proposal was reported in [17,27]. Very recently it has been proposed that mode stretching along with the use of a double cladding fiber can raise the sensitivity further when combining the effects of MT, TAP, and tunneling effect together [28].

Highly sensitive LPFGs were used in label-free biosensing applications [5–9]. Very recently an ultra-sensitive tantalum oxide coated LPFG-based biosensor was reported, where a highly sensitive LPFG operating near the DTP and the MT was used as a biosensor [29]. LPFG sensors were employed successfully for detection of butane gas [30], glucose [31], carbon dioxide [32], and streptavidin [33]. The specific coating is required for each of the application. Sol-gel coatings were

employed for identification of butane gas [30], ZIF-8/GO$_x$ were used for detection of glucose [31], metal-organic framework (HKUST-1) was useful for detection of carbon dioxide [31]. Over the past decade, distinct materials are coated over LPFG for the successful fabrication of biochemical sensor [3,29–33,5–9,and].

Therefore, nanomaterial coating is an essential approach for various sensitivity enhancement methods as described above in the case of designing ultrasensitive LPFG sensors for diverse chemical- and biosensing applications. However, a comparative study of the universal optimized design of nano-coating parameters is not available elsewhere. In this paper, a detailed numerical investigation is carried out to evaluate and optimize the performance of LPFG sensors with various coatings. Within chemical and biological sensing applications, the wavelength shift of the resonance is due to change in optical properties that occur near the surface of the sensor, where most of the biological/chemical reactions take place. Therefore, the response of the LPFG sensors strictly depends on that particular surface change in the context of the interaction of the receptor layer and the target analyte for fixed properties of a surrounding buffer medium (water/phosphate buffer saline, etc.). The volume refractive index sensitivity might not be adequate to define or interpret the sensitivity with respect to change in the surface of the sensors. Thus, the conventional definition of the RI sensitivity was modified to correspond more with specific biochemical applications, which occurred very close to the surface of the fiber sensor. Add-layer sensitivity was then introduced to quantified surface-based changes for coated LPFG. A multilayer-based architecture model was proposed elsewhere [34].

Requirements concerning multi-layer model of LPFG sensors are elaborated in earlier work [29,34]. A set of thin-film materials is required to be deposited on the surface of LPFG to reach high sensitivity. Sensitivity tuning overlay, bio-functional layer and receptor layers are required to be deposited on the surface of LPFG for specific immunoassay-based applications [7,9]. The schematic representation of the LPFG-based biochemical sensor has been shown in Fig. 2. (a). The Cross-sectional diagram of coated LPFG has been depicted in Fig. 2. (b). Side-view of multi-layer architecture for an immunoassay experiment has been given in Fig. 2. (c). In this paper, the performance of LPFG sensors has been reviewed critically for different coating materials and coating methodologies that have been investigated up to date. We focused here on sensitivity, limit of detection, and dynamic region of operation. In this work, it has shown that the performance of the sensor strongly depends on the RI of the overlay and its thickness. A slight change in deposited thickness may cause a drastic drop in the sensing performance of the sensor. The thin film deposition technique should be selected depending on the properties of the overlays to be deposited. For example, polymeric materials RI ~ 1.5–1.6 [3,13], where for sol-gel material ranges from 1.58 to 1.8 [6,15,21], and for metallic nano-particles and metallic oxides are it reaches 1.7–2 or even higher [29]. It
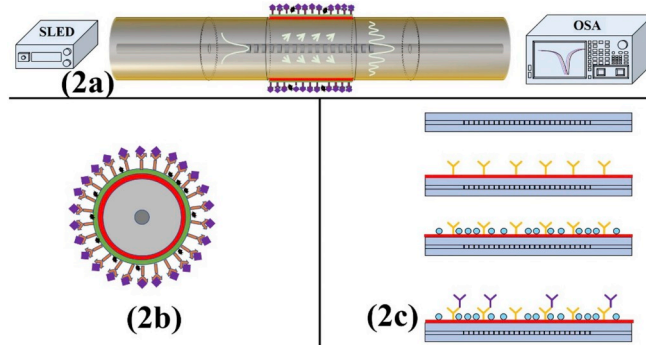

Fig. 2. (a) Schematic representation of LPFG structure. (b) Cross-sectional diagram of LPFG after a specific surface functionalization. (c) Side view of layered architecture model for immunoassay-based experiments.

is found from this work that the design of LPFG sensors must be case-specific and the performance of the sensors is not only countable on higher sensitivity. A recipe for the designing of the sensors is analyzed numerically.

The influence of overlay 'deposition techniques' and overlay materials on sensitivity, limit of detection and dynamic range of the sensors have also been studied in detail. This work will provide useful guidance to the design of LPFG sensors with higher values of overlay RI to achieve ultra-high sensitivity along with a superior limit of detection and large dynamic range of operation. It has been observed that design of the sensors must be case-specific otherwise meaningful detection will not be possible even with ultrahigh sensitive sensors. This proposed method will be a promising tool in case of designing FBGs with symmetric cladding modes [20], tilted FBGs [4] and cascaded optical fiber grating sensors [35,36].

2. Basic theory

Coupled mode theory is often used to study the properties of optical fiber grating-based sensors [37]. Transverse electric field components of the guided core or cladding modes propagating along the z-axis of the fiber gratings can be expressed by a generalized Eq. (1). The radial function $\Psi(r)$ of the individual layer of optical fiber can be written as in Eq. (1a)–(1b), where $k_0 = 2\pi/\lambda$ is the free space wavenumber, n is the refractive index of the layer, $\beta_{\upsilon j}$ is the longitudinal propagation constant of the $LP_{\upsilon,j}$ mode, and $\gamma_{\upsilon j} = \sqrt{[k_0^2 n^2 - \beta_{\upsilon,j}^2]}$ is the magnitude of the transverse wave number. $A_{\upsilon,j}$ and $B_{\upsilon,j}$ are the field expansion coefficients determined by the boundary condition of the cylindrical layers. $J_\upsilon(r\gamma_{\upsilon,j})$ and $Y_\upsilon(r\gamma_{\upsilon,j})$ are the ordinary Bessel function of the first and second kind, respectively, while $I_\upsilon(r\gamma_{\upsilon,j})$ and $K_\upsilon(r\gamma_{\upsilon,j})$ are the modified Bessel function of first and second kind of order υ, respectively.

$$\Psi(r, \theta, \Phi) = e^{-j\beta_{\upsilon j}z}\Psi(r)\Theta(\theta)\varphi(\phi) \tag{1}$$

$$\psi(r) = A_{\upsilon,j}J_\upsilon(r\gamma_{\upsilon j}) + B_{\upsilon,j}Y_\upsilon(r\gamma_{\upsilon j})\beta_{\upsilon j} < k_0 n \tag{1a}$$

$$\psi(r) = A_{\upsilon,j}I_\upsilon(r\gamma_{\upsilon j}) + B_{\upsilon,j}K_\upsilon(r\gamma_{\upsilon j})\beta_{\upsilon j} > k_0 n \tag{1b}$$

The optical guided modes in the core are being governed by Eq. (1a). Eq. (1b) is the characteristics equation of the cladding mode. The transfer matrix method [37,38] has been successfully applied to find out the effective indices of the modes and field expansion coefficients of multi-layer LPFG waveguide structure. Field expansion coefficients of each layer are normalized so that each mode carries the same power P_0, as in Eq. (2).

$$P_0 = \frac{\beta_{0j}}{2\omega\mu_0} \int_0^{2\pi} d\Phi \int_0^\infty \psi(r)\psi^*(r)r dr \tag{2}$$

2.1. Coupled mode formation for the waveguide structure

After the derivation of field expansion coefficients for each layer of the optical fiber, coupled-mode differential equations are formed assuming each of the forward propagating modes has complex amplitude $A(z)$ and neglecting backward propagating scattered wave [39,40]. The generalized coupled-mode equations are described in Eq. (3) for $\mu k = 01, \ldots\ldots M. K_{\upsilon j, \mu k}^t$ and $K_{\upsilon j, \mu k}^z$ are the transverse coupling and longitudinal coupling coefficients between $LP_{\upsilon j}$ and $LP_{\mu k}$ modes.

$$\sum_\upsilon \frac{dA_{\mu k}}{dz} = -j \sum_{\upsilon j=01}^M [K_{\upsilon j,\mu k}^t + K_{\upsilon j,\mu k}^z]A_{\upsilon,j}(z)\exp(-j(\beta_{\upsilon j} - \beta_{\mu k})z) \tag{3}$$

It is assumed that $K_{\upsilon j, \mu k}^t >> K_{\upsilon j, \mu k}^z$ so only transverse coupling coefficients are considered between the modes. Transverse coupling coefficients can be computed with the Eq. (4) prescribed in [37], where $\Psi_{\upsilon j}(r)$ and $\Psi_{\mu k}(r)$ are the transverse field components of $LP_{\upsilon j}$ and $LP_{\mu k}$ modes, respectively, $\Delta\varepsilon$ is the permittivity variation and is. It is defined

as $2n\Delta n$, where Δn is the change in the RI of the core during grating writing.

$$K_{\upsilon j,\mu k}^t = \int_{\Phi=0}^{2\pi} d\Phi \int_{r=0}^\infty \Delta\varepsilon\psi_{\upsilon j}(r)\psi_{\mu k}(r)r dr \tag{4}$$

2.2. Resonance wavelength

Resonance wavelength of a cladding mode can be found from the phase-matching condition given as $\beta_{01} - \beta_{0\upsilon} = \frac{2\pi}{\Lambda}$. The resonance wavelength of each cladding mode is given as $\lambda_{reso, m} = (n_{co}{}^{eff} - n_{cl, m}{}^{eff})\Lambda$, where $n_{co}{}^{eff}$ is the effective index of the core mode and $n_{cl, m}{}^{eff}$ are the effective indices of mth order cladding mode. For a change in the SRI, effective indices of the cladding modes are changed and a shift of the respective cladding mode can be observed in the transmission spectrum.

2.3. Add-layer sensitivity

The bulk or volume RI sensitivity of optical fiber grating-based structure is defined as a change in resonance wavelength of a particular cladding mode with respect to the SRI. If a change in resonance wavelength of mth cladding mode is defined as $\Delta\lambda_{reso, m}$, and change in SRI by Δn then the volume or bulk RI sensitivity is defined as $S_{\upsilon,m} = \frac{\Delta\lambda_{reso,m}}{\Delta n}$, S_υ is named as the bulk/volume RI sensitivity.

The add-layer sensitivity is defined for quantification of the surface-based changes during chemical and biological sensing applications with the LPFG sensor. Often the deposition of the mass of bio-analyte modeled as a thin layer over the surface of the sensors along with a characteristic density. With this assumption, one part of the add-layer sensitivity has been defined as the change of resonance wavelength ~ $\Delta\lambda_{reso, m}$ with respect to the thickness of an adsorbed layer on the surface of the specifically coated fiber, while it does not change in with SRI. This is the first part of the add-layer sensitivity (S_{TH}). The distinct coating provides the specific capture site for the target analyte. Often it has been observed that with an intake of target analytes in the form of gas/liquid molecules the RI of that capture site gets changed without any mass adsorption over the receptor molecules. This physical adsorption can be quantified with the second part of the add-layer sensitivity where the RI of that particular receptor layer close to the surface gets altered while the RI of the surrounding medium is remaining fixed throughout the experiment. This assumption leads to define other form of add-layer sensitivity in which the RI of the thin receptor layer is altered with the interaction of target analyte (S_{LRI}). The detailed definition and quantification of the add-layer sensitivity was illustrated in previous work [29,34]. Multilayer LPFG model was developed to establish this concept of add-layer sensitivity for LPFG sensor [34].

In summary, the add-layer sensitivity can be defined as in Eq. (5), where H_{AL} is the thickness of the added layer and n_{AL} is the corresponding RI of the layer.

$$S_A = \frac{d\lambda_{res}}{dH_{AL}} + \frac{d\lambda_{res}}{dn_{AL}} = S_{TH} + S_{LRI} \tag{5}$$

3. Numerical simulations

The parameters of the optical fiber for the analysis were similar to those of a standard commercially available single-mode fiber (SMF28-e Corning). RIs of the core and the clad have been chosen as $n_1 = 1.4494$ and $n_2 = 1.444$ (@ 1550 nm), respectively. Diameters of the fiber core and the clad were considered in turn as 8.2 μm and 125 μm, respectively. RI of the overlay was considered as n_3 (varied in a range 1.46–2.5) and that of the surrounding as $n_4 = 1.3333$ RIU (normal RI of water). The period of the grating was chosen to be 340 μm and RI perturbation in the core was selected as 0.0004. For the initial analysis,
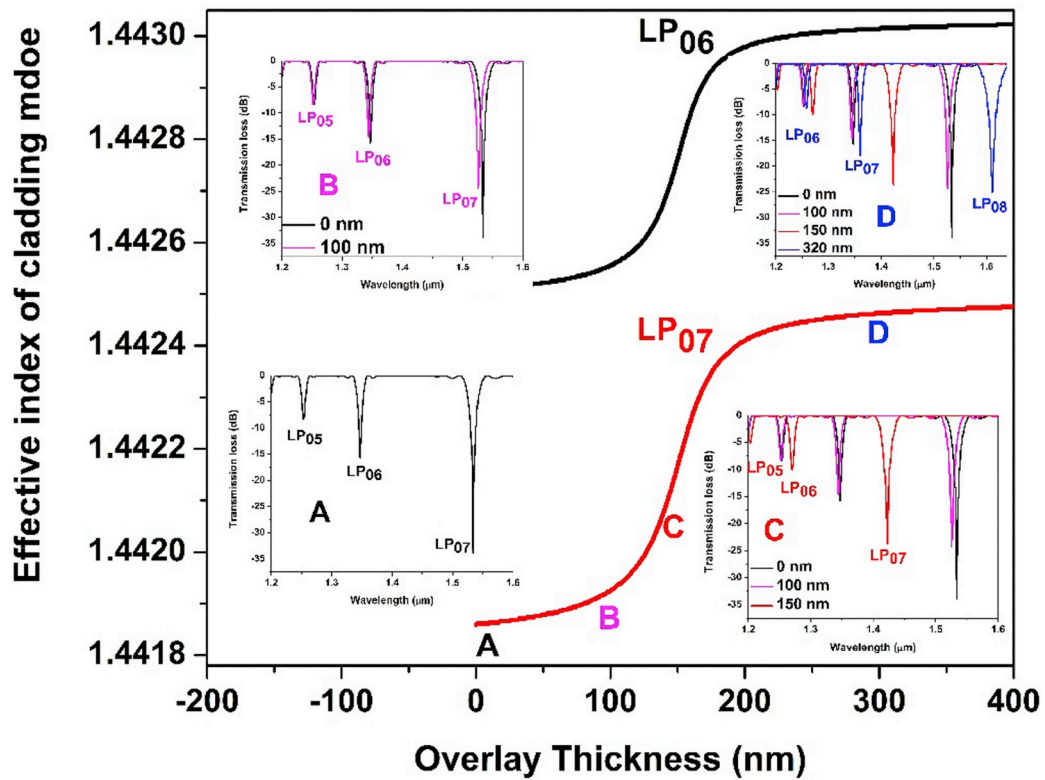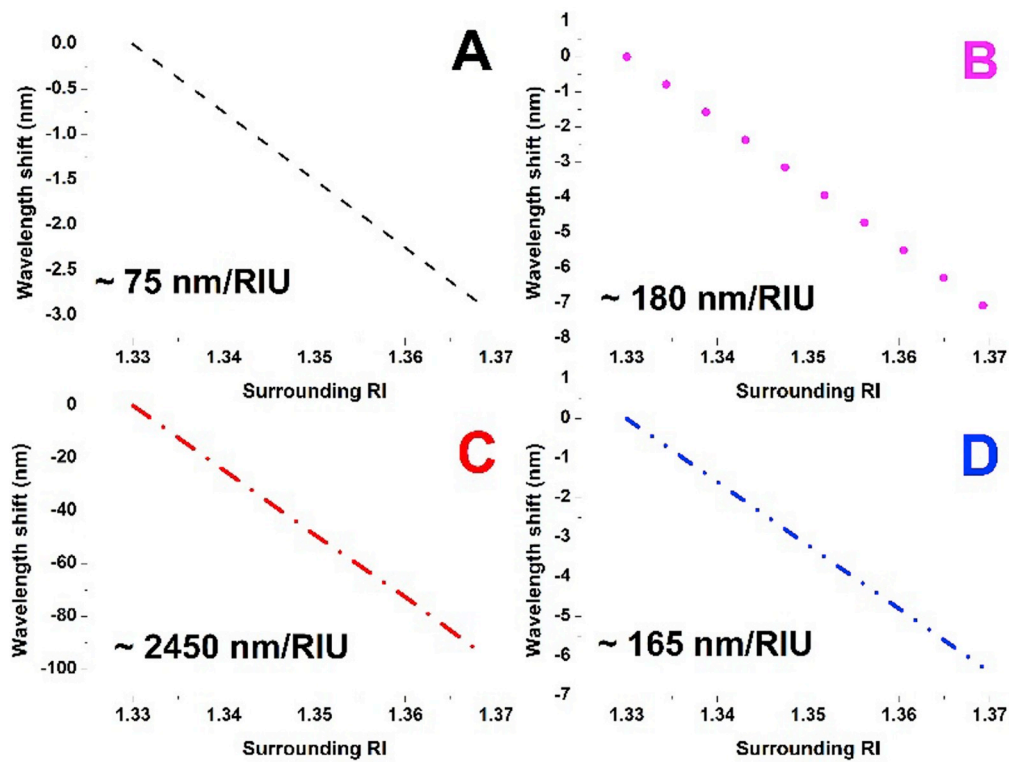
Fig. 3. (a). Mode transition curve of two cladding modes (LP_{06} and LP_{07}) with overlay thickness. Spectra of LPFG for different thickness of the overlay (point A, B, C and D) are given as inset. (b). Numerically computed sensitivity for LP_{07} cladding mode with change in SRI from 1.33–1.37 at different region in the MT curve and overlay thickness i.e., 'A'- 0 nm, 'B'-100 nm, 'C'-150 nm, and 'D'-320 nm.

the RI of the overlay was considered to be ~ 1.7 RIU. This value is similar to the silica-based sol-gel material [21]. Length of the grating for the entire simulation was considered 25 mm. The intention of these analyses was to understand the effect of MT with different RI of the overlay. Initially, a three-layer model (core-clad-surrounding medium) was assumed to evaluate the spectrum of LPFG to evaluate the spectrum with a specific grating period. A four-layer (core-clad-overlay-surrounding medium) model of LPFG was employed to simulate the effect of MT for two cladding modes (LP_{06} and LP_{07}) with a change in overlay thickness and is shown in Fig. 3(a). The variation of effective indices of two cladding modes with alteration of overlay thickness has been shown in Fig. 3a. The linear region of the MT curve can be observed in Fig. 3(a). Points 'A', 'B' 'C' and 'D' were marked as four different parts of the MT curve. The corresponding spectrum of LPFG have also been shown inset of Fig. 3(a) and they are being named as 'A' (overlay thickness ~ 0 nm), 'B' (overlay thickness ~100 nm), 'C' (overlay thickness ~ 150 nm) and 'D' (overlay thickness ~ 320 nm). Resonance band shifts of three cladding modes are depicted in the inset as four different spectrum, LP_{06} and LP_{07} modes are being identified in each of the inset figures. At point C, the attenuation band of LP_{07} (red) is in the middle of the initial LP_{06} and LP_{07} (black) position. The attenuation band of LP_{07} (blue) has almost reach the initial position of LP_{06} cladding mode and it represents a transition of cladding mode after deposition of that much of thickness (~320 nm) at position 'D'. The sensitivity for the two cladding mode was found to be significantly higher in position 'C' (~ 150 nm of overlay) which seems to be in the middle of the linear region of the curve. The volume RI sensitivity with different thickness of the overlay has been shown in Fig. 3(b). Optimum overlay thickness (OOT) was defined as the middle part of the highest slope region of the curve [13]. It has been found that the sensitivity with OOT was as high as ~ 2450 nm/RIU, where the sensitivity of the same cladding mode near 'A' was ~ 75 nm/RIU. Bulk/volume RI sensitivity was enhanced by ~ 30 times according to the results from these two positions of the thickness of overlay. The sensitivity at position 'D' is also quite low (~165 nm/RIU) since this position is far from the linear highest slope region of the curve. The OOT has also been defined as an operating point or alternatively Q-point of the sensor for that particular cladding mode in previously reported work. Distinct biological/chemical applications were verified by tuning operation of one specific cladding mode near the OOT/Q-point with significantly boosted the sensitivity for these experiments [6,21,29].

The change in the effective index of a particular cladding mode (LP_{07}) with overlay thickness has been shown in Fig. 4(a). OOT and linear region have been marked. The highest slope position is termed as the "linear region" of operation, where the sensitivity of the respective cladding mode is maximum. The linear span region of LP_{07} cladding mode with an overlay RI of ~ 1.7 RIU is ~ 60 nm (115 nm–175 nm of overlay thickness) and the OOT/Q-point of respective LP_{07} cladding mode is being found at ~ 150 nm. The computed OOT matches the maximum sensitivity for previously performed experiments where similar silica-based sol-gel material was used for reaching MT [21]. The variation of the MT curve of LP_{07} cladding mode with different overlay RI (1.6 to 2.5 RIU) has been shown in Fig. 4(b). The 'linear region' of operation and 'Q-point' are both shifted with the change in overlay RI. The variation of the effective index of the cladding mode with overlay RI near to cladding (i.e. RI ~ 1.45) has been shown in the supplementary Fig. S1, where it can be observed that OOT is as high as ~ 2000 nm with an overlay RI of ~ 1.45. Variation of OOT/Q-point and sensitivity of LP_{07} cladding mode with different RI of overlay has been computed and results are shown in Fig. 5(a). It is worth noting that sensitivity and OOT change promptly with overlay RI. Variation of the range of" linear region" of operation of the MT curve for different RI of overlay has been depicted in Fig. 5(b). It was observed that the higher the overlay RI is, the higher the sensitivity and narrower the "linear zone" of operation for the respective cladding mode. Simulated sensitivity of LP_{07} cladding mode with overlay RI 1.6 is found to be ~1500 nm/RIU, for OOT ~ 350 nm and linear region ~ 75 nm. Numerically computed sensitivity of the respective cladding mode is ~ 8000 nm/RIU for overlay RI ~2, but OOT and 'linear region' of operation are only ~ 66 nm and ~ 27 nm, respectively. The 'linear region' of operation is shortened drastically with higher RI of the overlay. In case of determination of change of SRI, the phenomena of "lowering down of linear zone" will not affect at all but for the measurement of surface-based changes, it has some serious effect which has been described below. The dynamic range of the sensor affects enormously with the change in "linear zone" of operation. Appropriate bio-functional layer (BFL) and receptor layers (RL) are required to be deposited over the surface for specific detection of target with highly sensitive overlay coated LPFG. An BFL normally acts as a buffer layer between the glass/polymeric surface and bio-material based RL. Then a specific RL (distinct biolayer for specific attachment of bio-analyte) needs to be deposited before attachment of target analyte to provide sufficient capture
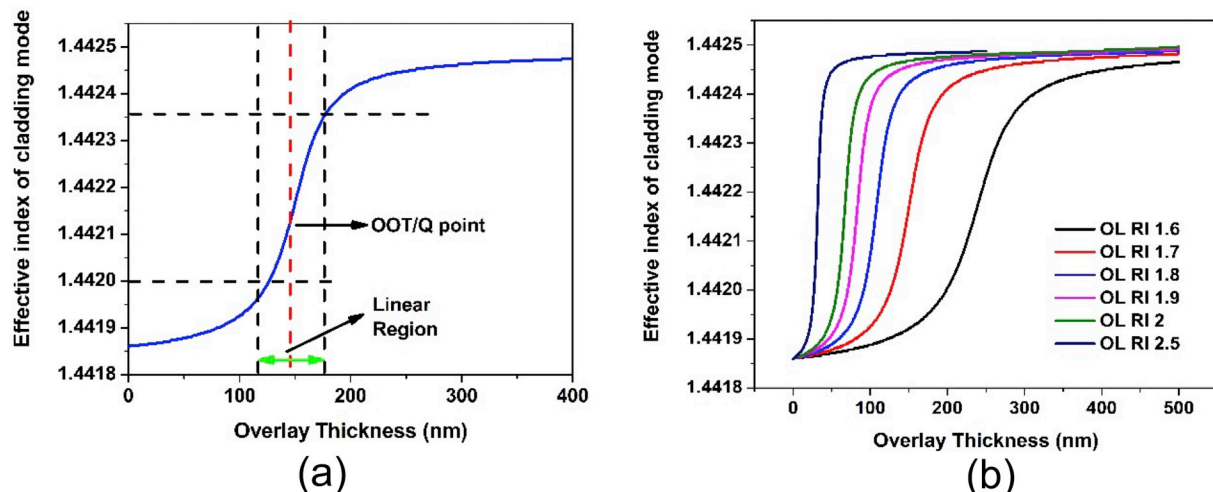

(a)

(b)

Fig. 4. (a) Variation of effective index of cladding mode with overlay (1.7 RIU); (b) Variation of mode transition curve for different RI of the overlay materials.
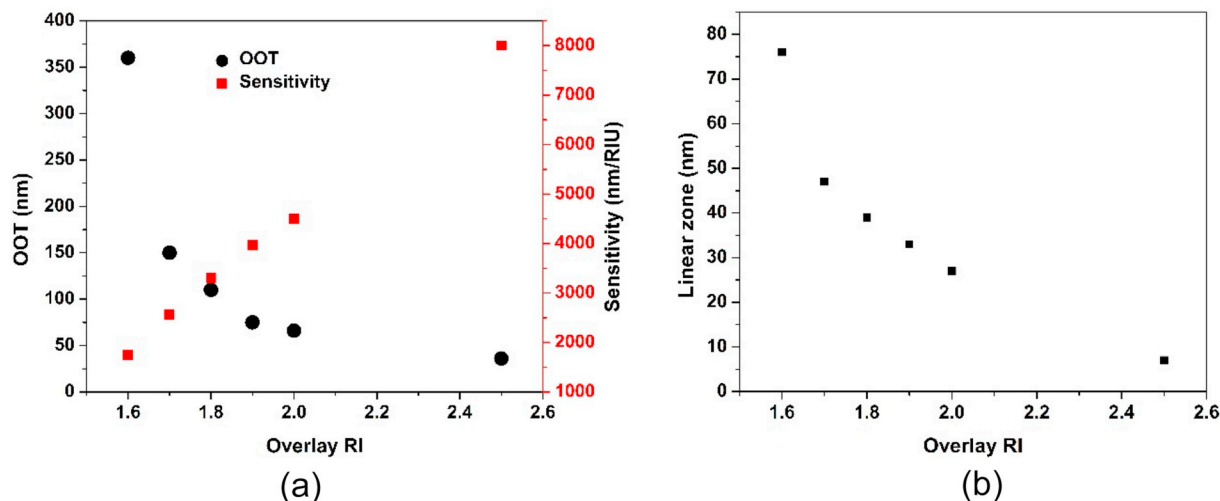
Fig. 5. (a) Variation of sensitivity and OOT with different values of overlay RI. (b) Change in span of linear zone of the operation of LP_{07} cladding mode with different overlay RI.

sites for acceptance of the target specimen [6–8,21]. The effect of MT with consideration of two different thin layers BFL and RL of different thickness) have been analyzed critically. The RI of BFL has been chosen to be 1.54 [13,18,19] and the RI of the receptor layer was chosen as 1.5 for the analysis as RI of the dry protein is in the range of 1.4–1.6 [41]. The thickness of the bio-functional layer is kept at 5 nm for the purpose of computations. This value of the BFL was numerically computed elsewhere and was validated with experimental outcome [34]. Thickness of BFL and RL can vary in a wide range (few nm to a few hundred nm depending on bio-material/species concern). Diverse type of biomolecules possesses different thickness along with distinct values of RI [3,34,41]. The RI of the overlay for the numerical analysis has been now been increased to ~ 2 for the next part of the simulation of the paper, as the design aim is to reach the higher sensitivity with a change in SRI and RI ~ 2 can be achieved practically [21,23,29].

Fig. 6(a) shows the effect of BFL and RL over the MT curve for LP_{07} cladding mode. It should be mentioned that BFL is always kept at 5 nm for this numerical study. The effect of the influence of RL has been computed with a complete six-layer LPFG model (core-clad-OL-BFL-RL-Surrounding medium). The positions of operating point for different thickness of RL with a fixed BFL of (5 nm) has been shown in Fig. 6. Considering the effects of BFL and RL, the OOT shifts abruptly from the most sensitive point. Without any BFL and RL, the OOT has been marked as Q1. The simulated value of OOT has been come up to ~ 66 nm with an overlay RI of ~ 2. The operating point has been shifted to Q2, Q3, Q4, and Q5 depending on the thickness of deposited RL (with a thickness of 10 nm, 20 nm, 50 nm, and 100 nm). The sensitivity of LPFG in the position Q2 and Q3 is almost the same as that of original operating point Q_1 but that of in position Q4 and Q5 is drastically lower than the operating point of Q_1. Position Q4 and Q5 are far from the sensitive linear point and as an immediate effect volume RI sensitivity and Add-layer sensitivity were truncated massively. This abrupt reduction of sensitivity with deposition of BFL (~ 5 nm) and RL (~ 50 nm/100 nm) above the surface of an overlay of ~ 66 nm makes the sensors inappropriate for sensing applications. This specific sensor can achieve high sensitivity with a change of overlay thickness to accommodate the RL and BFL for specific applications., the deposited thickness of the overlay must be modulated as per the thickness of BFL and RL to achieve the best performance of the sensor. The OOT of the individual sensors must be tuned by the thickness and RI of BFL and RL. It is apparent that with the deposition of BFL and RL the effective index of the cladding mode changes and the operating point gradually moves out of the most sensitive linear zone. The change of volume RI sensitivity and the add-layer sensitivity with consideration of BFL and RL
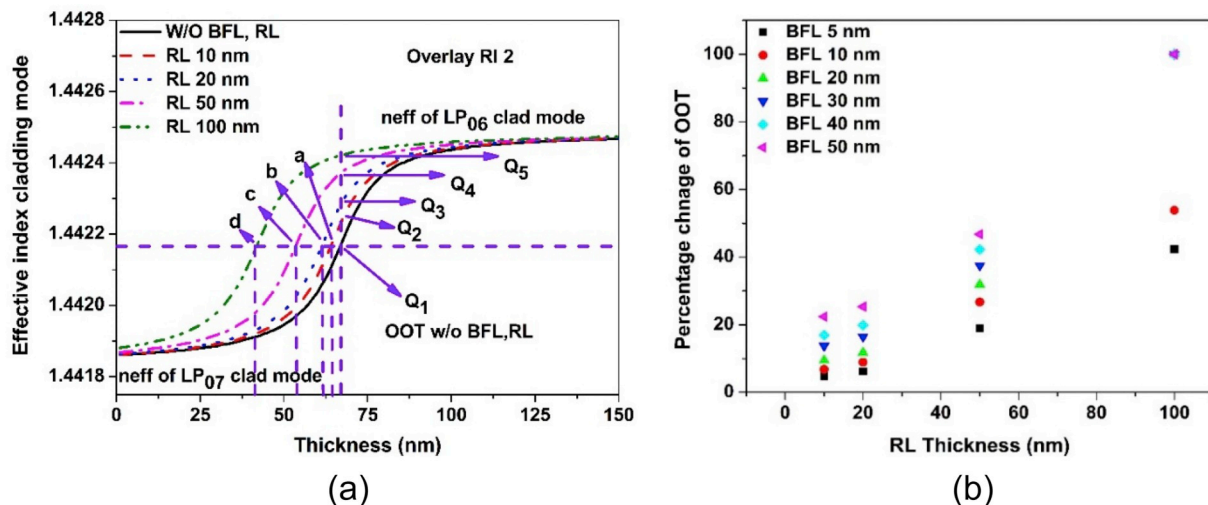

Fig. 6. (a) Variation of MT curve with different thickness of RL, keeping BFL thickness fixed to 5 nm. (b) Numerically computed results showing percentage of variation of OOT with RL thickness for different bio-functional layer.

were given in recently published work [29,34]. The variation of volume RI sensitivity and add-layer sensitivity with the presence of BFL and RL has been shown in Fig. S2 and Fig. S3 in the supporting document. Simulated OOT for LP_{07} cladding mode with an overlay of RI ~ 2 and without consideration of BFL and RL was found to be ~ 66 nm and it should be modulated to ~ 63 nm, ~ 57 nm, ~ 53 nm, and ~ 41 nm to adopt a BFL of 5 nm along with RL of 10 nm, 20 nm, 50 nm, and 100 nm, respectively. It should be mentioned that the influence of the RL was computed assuming a BFL thickness of 5 nm. Fig. 6. (b) shows a change in the percentage of required deposition of OOT to attain the maximum sensitivity for different thicknesses of RL with a few tens of nm of BFL. The reported thickness of small receptor molecules like few tens of base pairs of DNA strands, antibodies, biotins, etc. was from a few nm to a few tens of nm. The thickness of virus/bacteria/large protein molecules with a long amino acid chain can be varied from a few tens of nm to ~ hundreds of nm or even couple of μm. It must be noted that functionalized nanoparticles were used together with RL and BFL for the designing of biochemical sensors [42]. The size of the specifically functionalized nanoparticles can be varied from tens of nm to hundreds of nm. The most sensitive point of the cladding mode of LPFG can be ensured with an alteration of the deposited thickness of overlay to accommodate the required space for BFL and RL. Detailed computation shows a change in the percentage of required OOT to accomplish the finest performance was 4.76%, 9%, 18.9% and 42.4% with different thickness of RL. Six sets of different thickness of BFL (5, 10, 20, 30, 40 and 50 nm) were considered for this computational work. The results show that the change in percentage of required thickness of OOT must be 9%, 22%, 46% and 74% with 10, 20, 50 and 100 nm of RL with a BFL of 20 nm. The change in percentage of OOT with different thickness of RL for a particular thickness of BFL has been shown in Fig. 6. (b). Use of overlay with higher RI makes it possible to achieve higher sensitivity, but to operate the specific cladding mode in the best sensitive range one should precisely determine the RI and thickness of the deposited overlay and bio-materials i.e., BFL and RL. In all of the above results are observed with the surrounding medium close to that of water (RI ~ 1.3333). Bio-chemical sensing procedures are normally carried out in the water or other specific buffer solutions. Phosphate buffer saline (PBS) [pH ~ 6–8] are mostly used buffer solutions, but many potential applications are being carried out within Citrate buffer (pH ~ 3 to 6.5) and Acetate buffer (pH ~ 3 to 6.5) solutions as per the requirement of application domain and scope. The RI of the PBS ~ 1.335, measured RI of the Acetate buffer is ~ 1.344 and that of Citric acid buffer is ~1.362. The variation of the MT curve of the LP_{07} cladding mode with a change in the surrounding medium has been shown in Fig. 7. (a) below. The Q point of the sensor has been shown as Q1, Q2,

Q3, and Q4 in the graph, Q1, Q2 = ~ 66 nm, Q3 = 62 nm, and Q4 is found to be ~ 57 nm respectively. The OOT of specific cladding mode of LPFG changes significantly with the change in RI of buffer solution with the same overlay material. As the RI of water and PBS are same there is no significant change of OOT for these two-surrounding medium, but with an application of the other two buffers, the OOT changes and this change must be taken into account during the designing of biosensors. Otherwise, the performance of the sensor will be degraded. Another important observation is that the calculated values of the 'linear zone' of operation have been changed to ~ 17 nm in the case of Citrate buffer solution from a linear zone of 27 nm with a surrounding medium as water/PBS. As a consequence, the dynamic range of the operation of the sensor will also be affected by changing the surrounding buffer medium. The percentage change in OOT to achieve optimum performance with 5 nm of BFL and four different thicknesses of RL in different buffer medium were simulated. The variation of change in percentage of OOT with thickness of RL has been shown in Fig. 7. (b). Variation of add-layer sensitivity with different buffer medium after deposition of OOT in water medium has been given in supplementary Fig. S4 and Fig. S5. In summary, fine-tuning of the deposited overlay layer is necessary to improve the performance of the sensor for different buffer medium. The detailed discussion of performance of LPFG based biochemical sensors with an enhancement of sensitivity, lowering down of linear region of operation are illustrated in the next part of this work.

4. Discussions

4.1. Sensitivity and limit of detection

Volume RI sensitivity of LPFG sensors with an overlay RI of 2 is about ~ 8000 nm/RIU in an SRI zone of (1.333–1.36). Detailed discussion of add-layer sensitivity along with adhesion of bio-layer and with change in surface RI was reported elaborately in our earlier work [29,34]. The limit of detection (LOD) of the sensor directly depends on the add-layer sensitivity. With varying the concentration of target analyte, the deposited nanolayer thickness of the surface changes as the concentration modulates the deposited mass of the analyte over the sensing head [43,44]. A very low LOD can be achieved with higher add-layer sensitivity. Previously proposed methods like mode stretching, utilization of double-clad fiber (combining of tunneling effect with MT), merging the effect of MT and DTP of cladding mode can enhance the add-layer sensitivity significantly to be as high as ~ 20/25 nm shift in resonance wavelength per nm attachment of bio-layer over the surface of the sensor. With an interrogation system of resolution of ~ 20 pm, which is readily available for any standard commercial detector,
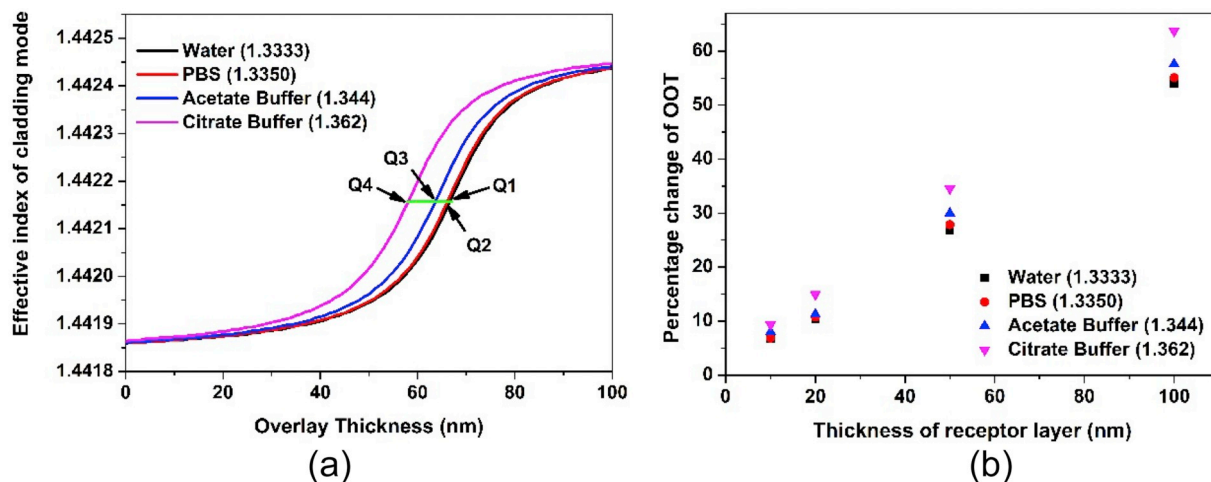

Fig. 7. (a) Numerically computed MT curve of LP_{07} cladding mode for different surrounding buffer region with overlay RI = 2. (b). Percentage change of OOT with 5 nm BFL, 10 nm RL for different buffer medium.
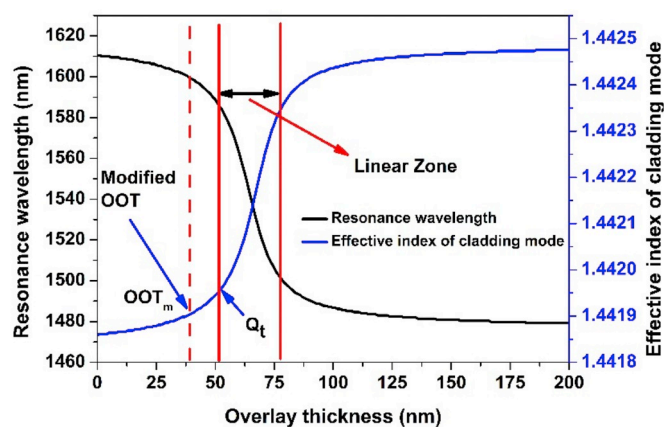
Fig. 8. Variation of resonance wavelength (nm) and effective index of LP_{07} cladding mode with deposition of overlay thickness (RI = 2).

adhesion of less than ~ 1 picometer thickness of target analyte above the surface of LPFG might be detected. If properly designed, a femto-molar concentration of specific antigens/DNA strands can be identified for immunoassay/DNA sequencing-based applications. There is a bottleneck problem of the dynamic range of the sensor with enhancement of the sensitivity and LOD and it will be discussed in the next section.

4.2. Dynamic range of the sensor

Bio-assay based experiments are normally accomplished including identification of different concentration of target analytes to assess the performance of the sensors. The dynamic range of the biochemical sensors is defined as the range of the concentrations of the target analyte that can be recognized by the sensors. Deposited bio-film thickness of the target analyte normally depends on the nature of the species and concentration of the solution. The dynamic range of LPFG-based sensors depends on the linear zone of operation of the MT curve. Higher the sensitivity, narrower is the linear zone of operation. As a comparison, linear zones of the LPFG with OL RI of 1.7, 2 and 2.5 are ~ 48 nm, ~ 27 nm, and ~7 nm respectively. With conventional definition, OOT/Q point is the middle portion of the linear operation zone. As an immediate effect, the linear span remaining for bio-functionalization is effectively reduced to ~ 24 nm, ~13.5 nm and ~3.5 nm with overlay RI 1.7, 2 and 2.5 respectively. BFL, RL and respective target analyte are required to be accommodated within this linear span to achieve the prime performance of the sensors. Computed add-layer sensitivity of LP_{07} cladding mode is ~ 2.2 nm, 4.74 nm and ~8.82 nm/ (nm attachment of bio-analyte layer) with overlay RI of 1.7, 2 and 2.5, respectively. So, with overlay, RI reaching 1.7 and conventional design method only ~ 10.90 nm attachment of RL, BFL, and target analyte can be possible with overlay RI 1.7 (linear zone/add-layer sensitivity; 24/2.2 = ~ 10.90). The scenario becomes much more challenging as for overlay RI reaching 2 and 2.5, only ~ 2.85 nm and ~ 0.4 nm attachment of biolayer can be accommodated in the high sensitivity zone. That means the bio-immunoassay experiment reported in [21] where a sol-gel Silica-Titania film of RI (~ 1.69) as an overlay for the detection of specific anti IgG was never possible with OL of RI 2 or 2.5 with conventional definition of OOT/Q-point. After deposition of the Eudrajit layer as BFL (thickness ~ 5 nm) and IgG as RL (~ 10 nm of thickness) above an OOT the cladding mode shifts from the most sensitive point in case of overlay RI 2 and 2.5. There will be no significant amount of wavelength shift with deposition of antigen (target molecules) as after attachment of BFL and RL the cladding will be shifted from the highly sensitive linear zone. So, the enhancement of the sensitivity of LPFG might not always be the key criterion for designing efficient sensors. The size of the bio-analyte must be considered during design and fabrication of the sensing device. Thickness of overlay, BFL

and RL need to be adjusted properly to achieve the best performance during the detection of the target analyte. Ellipsometry based measurements had confirmed that thickness of a single bacteria can be of few hundreds of nanometers with an RI value of 1.4–1.6 [45]. RI of the deposited bacteria layer was evaluated with the filling fraction of bacteria within the thin film as per Maxwell- Garnett approximation and came up to about ~ 1.5 [46]. The measurement of mass, thickness, and density of ram spermatozoa and T2 Bacteriophage was measured successfully by Electron Microscope with Mass-Thickness model [47]. Thickness of thiol modified DNA strands adsorbed over the surface of the sensor and was evaluated with atomic force microscopic based measurements. The deposited thickness of DNA strands was nearly ~ 6 nm, the values of deposited thickness of the synthetic DNAs can be higher as the length depends on the number of base pairs that have been used for the construction of DNA. The thickness of DNA layers can be varied from nm to a couple of tens of nm [48]. Most of the mammal cell possesses the thickness in µm range, like the size of the single red blood cells, is about few µm [49]. For selective detection of the target analyte typically a specific bio-receptor layer is requiring to be deposited over the sensor surface. Bio-compatible polymers like polystyrene and Eudrajit are used extensively with this family of sensors [6,21]. Gold nanoparticles are used as a universal receptor for numerous biological/chemical target species [43]. Different Size of the receptor layers (from few nm to 100 nm) can be fabricated with gold nanoparticles/ gold nanorods etc. [43,50,51]. In this discussion, it can be concluded that designing strategy of highly sensitive LPFG sensors will be decidedly dependent on the thickness and RI of the bio-materials. It has also been observed that with the conventional concept of OOT, the dynamic range of operation of the sensors decreases very rapidly with higher RI values of the overlay. In the next sub-section, an efficient designing method of LPFG has been proposed.

4.3. Proposed designing method procedure

Most of the linear zone of highly sensitive sensors can be used, but the deposited thickness of the overlay must be kept below the start of the linear zone of the MT curve for a specific order of the cladding mode. In Fig. 8 it has been shown as 'OOT$_m$', it is a point in the MT curve where the slope of the curve is low. The total linear regime (~ 27 nm) of highly sensitive sensor of LPFG with overlay RI of 2 can be used for deposition of RL/BFL and finally, respective cladding mode is at the best sensitive position before a specific biochemical application at 'Q$_t$'. The Volume RI sensitivity and add-layer sensitivity are very low at the point 'OOT$_m$' marked in the MT curve for LP_{07} cladding mode. Computed volume RI sensitivity was found to be ~ 300 nm/RIU and add-layer sensitivity (Sa) was ~ 0.61 nm per attachment of an nm of overlay layer (RI ~ 2). After deposition of 5 nm BFL and 10 nm RL the cladding mode reaches the point 'Q$_t$' which is the starting point of most sensitive region with a span of ~ 25 nm. In this way, the whole linear highly sensitive zone is being kept open to accommodate target-analyte with different sizes and RI. This point 'Q$_t$' is optimal for specific biochemical sensors. Here the position of 'Q$_t$' point reflects the incorporation of 5 nm BFL (RI~ 1.54) and 10 nm RL (~ RI 1.5). With a change in thickness and RI of BFL and RL, this 'Q$_t$' point will be changed. However, in the case of design, there will be a challenge to deposit accurate value of the overlay material up to 'OOT$_m$' as the shift of resonance cladding mode will be extremely low with the deposited thickness of overlay. So, tolerance will be invaded immediately in case of specific designing. Till now, the deposited value of overlay material is being optimized with a recorded shift of specific cladding mode, but in this new concept will be no significant shift of cladding mode up to the point 'OOT$_m$' of the MT curve as shown by the black curve in Fig. 8. In this scenario three techniques can be used for the optimization, a) idea from simulated curve with particular RI of used materials b) measurement of the cross-section of the fiber with electron microscopy and c) optimization of the rate (deposited thickness of overlay in nm/s)

of the deposition method to ensure the appropriate deposition of an overlay. Certainly, the deposition method plays a crucial role in case of the development of the sensor with higher RI overlay. With a close investigation of Fig. 8, it has been found that from 0 to ~ 38 nm of deposited overlay computed shift of resonance wavelength of the respective cladding mode was ~ 6 nm. It seems that the technique comprises the higher resolution of deposited thickness and must be a good choice for designing efficient sensors. Different techniques of deposition of overlay have been discussed elaborately. Accuracy of the deposition techniques will be immensely important in the case of designing the sensors with higher overlay RI as error of deposition of few tens of nm can degrade the performance of the sensor in a serious way.

Various coating methodologies have been adopted to deposit thin film over surface of the optical fiber grating-based sensors during the last one and a half-decade. Among them, electrostatic self-assembly (ESA), layer by layer thin film coating (LBL) [13,19], Langmuir Blodgett method (LB) [18], dip-coating technique [6], atomic layer deposition (ALD) [5], plasma-enhanced chemical vapor deposition (PECVD), plasma vapor deposition (PVD), thermal evaporation, sputtering techniques, and chemical growth methods are mostly used processes for the deposition purpose [1–4,17,]. A very good review was reported where the merits or demerits of each of the processes were described nicely in [52]. A detail aspect of all the deposition techniques was also elaborated elsewhere [52,53]. Resolution of the deposited thickness is immensely important for designing accurate sensors and lower resolution thickness of deposition is mandatory for the materials with having RI > 2. Among all the processes ALD method will be a choice while working with material over RI > 2 as the resolution of ALD is < 1 nm. In case of deposition of a few hundred nm of material (with overlay RI < 1.7) deposition with ALD is not optimal as it takes much time for the deposition purpose. In the case of polymeric material, it has been observed that ESA is much more suitable than ALD and a dip-coating method. Thermal/e-beam evaporation is useful for the deposition of the metal layer over the fiber surface. Materials are also imposing a limitation on the selection of deposition techniques. A schematic representation of coating methods with a range of RI material and resolution is given above in Fig. 9.

In case of developing immunoassay, DNA or protein sensors, a shorter linear zone might not affect that much with overlay RI < 1.7, but in case of detection of bacteria, viruses, biological cells one should ensure the dynamic range of the sensors must accommodate with the linear region of the effective index curve of cladding modes. Case-specific designing techniques are required to design and fabrication of this sensor in various chemical and biological sensing applications. Materials for overlay coating, coating methodologies, and OOT must be selected with consideration of following factors: a) RI of the overlay layer (required to achieve adequate sensitivity) b) the size of the target analyte c) modal characteristic of the respective fiber d) deposition time of the coating technique.

5. Conclusion

In this paper, an extensive numerical work has been carried out to assess design criteria for the fabrication of highly sensitive LPFG based sensors for selective chemical and biological sensing applications. It has been established that the MT effect of cladding modes is one of the most widely used methodologies to achieve high sensitivity in the case of LPFG sensors. Other methodologies like operating the cladding mode near TAP/dispersion turning point, modal stretching and deposition of nanoparticles/graphene/carbon nanotube-based 2d materials are also combined with MT effect to enhance the sensitivity further. Higher sensitivity with MT effect imposes a real challenge for the adequate dynamic range of the sensors, which has also been discussed elaborately in this work. In the case of designing an LPFG sensor, the selection of the deposition techniques has been analyzed in terms of sensitivity and dynamic range of the sensor. Deposition technique with a lower value of resolution in deposited thickness became an ultimate choice for deposition of higher RI overlay to ensure effective operation along with a high dynamic range of sensor. The relationship between dynamic range, the limit of detection and sensitivity of LPFG sensors have been analyzed critically in this work. The concept of OOT has been redefined according to use of full dynamic range and superior add-layer sensitivity. A detailed comparative study has been given in the discussion section. In summary, it has been observed that achieving the highest sensitivity is not the solitary merit when designing and fabricating of LPFG sensors. Designing of LPFG based sensors must be target-specific, and one needs to have at least some knowledge about the size and shape of the receptor, bio-functional specimens, and target molecules. Without having an estimation of these parameters, designing of highly sensitive sensors will be very difficult and many cumbersome trials will be required to operate the sensors at best sensitive region. The effect of buffer medium also needs to be considered to achieve an efficient performance. Optimization technique of nanocoating methodologies to achieve superior performance of LPFG can also be used in case of designing highly sensitive biosensors with fiber Bragg grating, tilted fiber grating, and cascaded optical fiber sensors.

Authors contribution

Conception and design of study: Sankhyabrata Bandyopadhyay, Liyang Shao, Mateusz Smietana, Chao Wang.

Acquisition of data: Sankhyabrata Bandyopadhyay, Jie Hu, Liu Shuaiqi.

analysis and/or interpretation of data: Sankhyabrata Bandyopadhyay. Mateusz Smietana,Liyang Shao,

Drafting the manuscript: Sankhyabrata Bandyopadhyay, Mateusz Smietana, Chao Wang, Liyang Shao.

Revising the manuscript critically for important intellectual content: Wu Qiang, Guoqiang Gu, Yanjun Liu, Xiaolong Chen, Zhangqi Song, Xuefeng Song, Qiaoliang Bao.

Approval of the version of the manuscript to be published (names of all authors must be listed): Sankhyabrata Bandyopadhyay, Liyang Shao, Chao Wang, Liu Shuaiqi, Wu Qiang, Guoqiang Gu, Jie Hu, Yanjun Liu, Xiaolong Chen, Zhangqi Song, Xuefeng Song, Qiaoliang Bao and Mateusz Smietana.
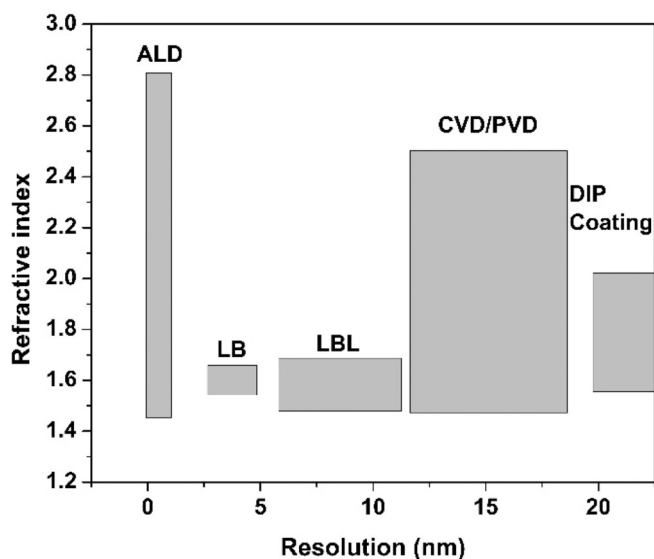
Fig. 9. Schematic representation of different coating methodologies with RI range and resolution thickness.

Declaration of Competing Interest

The authors declare no conflict of interest.

Acknowledgment

Appendix A. Supplementary data

Supplementary data to this article can be found online at https://doi.org/10.1016/j.sbsr.2019.100320.

References

[1] X. Wang, O.S. Wolfbeis, Fiber optic chemical sensors and biosensors (2008-2012), Anal. Chem. 85 (2) (2013) 487–508, https://doi.org/10.1021/ac303159b.

[2] X. Wang, O.S. Wolfbeis, Fiber optic chemical sensors and biosensors (2013-2015), Anal. Chem. 88 (1) (2016) 203–227, https://doi.org/10.1021/acs.analchem.5b04298.

[3] F. F Chiavaioli, S. Baldini, C.T. Tombelli, A. Giannetti, Biosensing with optical fiber gratings, J. Nanophotonics 6 (4) (2017) 663–679, https://doi.org/10.1515/nanoph-2016-0178.

[4] J. Albert, L. Shao, C. Caucheteur, Tilted Fiber Bragg grating Sensors, Laser Photonics Rev. 7 (2013) 83–108, https://doi.org/10.1002/lpor.201100039.

[5] E. Brzozowska, M. Koba, M. Smietana, S. Gorska, M. Janik, A. Gamian, W.J. Bock, Label-free gram-negative bacteria detection using bacteriophage-adhesin-coated long-period gratings, Biomed. Opt. Express. 7 (3) (2016) 829–840, https://doi.org/10.1364/BOE.7.000829.

[6] P. Pilla, P. Foglia Manzillo, V. Malachovska, A. Buosciolo, S. Campopiano, A. Cutolo, L. Ambrosio, M. Giordano, A. Cusano, Long period grating working in transition mode as promising technological platform for label free biosensing, Opt. Express 17 (22) (2009) 20039–20047, https://doi.org/10.1364/OE.17.020039.

[7] F. Chiavaioli, P. Biswas, C. Trono, S. Bandyopadhyay, A. Giannetti, S. Tombelli, N. Basumallick, K. Dasgupta, F. Baldini, Towards sensitive label-free immunosensing by means of turn-around point long period fiber gratings, Biosens. Bioelectron. 60 (15) (2014) 305–310, https://doi.org/10.1016/j.bios.2014.04.042.

[8] M. Koba, M. Smietana, E. Brzozowska, S. Gorska, P. Mikulic, W.J. Bock, Reusable bacteriophage adhesin-coated long-period grating sensor for bacterial lipopolysaccharide recognition, IEEE J. Lightw. Technol 33 (12) (2015) 2518–2523, https://doi.org/10.1109/JLT.2014.2364118.

[9] C. Liu, B.J. Xub, L. Zhou, Z. Sun, H.J. Mao, J.L. Zhao, L. Zhang, X. Chen, Graphene oxide functionalized long period fiber grating for highly sensitive hemoglobin detection, Sensor Actuat B-Chem 261 (2018) 91–96, https://doi.org/10.1016/j.snb.2018.01.117.

[10] V. Bhatia, A.M. Vengsarkar, Optical fiber long period gratings sensors, Opt. Lett. 21 (9) (1996) 692–694, https://doi.org/10.1364/OL.21.000692.

[11] H.J. Patrick, A.D. Kersey, F. Bucholtz, Analysis of the response of long period fiber gratings to external index of refraction, IEEE J. Lightw. Technol. 16 (9) (1998) 1606–1612, https://doi.org/10.1109/50.712243.

[12] X. Shu, L. Zhang, I. Bennion, Sensitivity characteristics of long-period Fiber gratings, IEEE J. Lightw. Technol. 20 (2) (2002) 255–266, https://doi.org/10.1109/50.983240.

[13] I. Del Villar, I.R. Matias, F.J. Arregui, P. Lalanne, Optimisatiom of sensitivity in long period fiber gratings with overlay deposition, Opt. Express 13 (1) (2005) 56–69, https://doi.org/10.1364/OPEX.13.000056.

[14] I. Del Villar, Ultrahigh-sensitivity sensors based on thin-film coated long period gratings with reduced diameter, in transition mode and near the dispersion turning point, Opt. Express 23 (7) (2015) 8389–8398, https://doi.org/10.1364/OE.23.008389.

[15] P. Pilla, C. Trono, F. Baldini, F. Chiavaioli, M. Giordano, A. Cusano, Giant sensitivity of long period gratings in transition mode near the dispersion turning point: an integrated design approach, Opt. Lett. 37 (19) (2012) 4152–4154, https://doi.org/10.1364/OL.37.004152.

[16] P. Biswas, N. Basumallick, S. Bandyopadhyay, A. Ghosh, K. Dasgupta, S. Bandyopadhyay, Sensitivity enhancement of turn-around-point long period gratings by tuning initial coupling condition, IEEE Sensors J. 15 (2) (2014) 1240–1245, https://doi.org/10.1109/JSEN.2014.2361166.

[17] M. Smietana, M. Koba, P. Mikulic, W.J. Bock, Combined plasma-based Fiber etching and diamond-like carbon Nano-overlay deposition for enhancing sensitivity of long-period gratings, IEEE J. Lightw. Technol. 34 (19) (2016) 4615–4619, https://doi.org/10.1109/JLT.2016.2528411.

[18] N.D. Rees, S.W. James, R.P. Tatam, G.J. Ashwell, Optical fiber long-period gratings with Langmuir-Blodgett thin-film overlays, Opt. Lett. 27 (9) (2002) 686–688, https://doi.org/10.1364/OL.27.000686.

[19] Z. Wang, J.R. Heflin, K. Van Cott, R.H. Stolen, S. Ramachandran, S. phase-matching, Biosensors employing ionic self-assembled multilayers adsorbed on long-period, Sensor Actuat B-Chem 139 (2) (2009) 618–623, https://doi.org/10.1016/j.snb.2009.02.073.

[20] S. Bandyopadhyay, T. Dey, N. Basumallick, P. Biswas, K. Dasgupta, S. Bandyopadhyay, High sensive Refractometric sensor using symmetric cladding modes of an FBG operating at mode transition, IEEE J. Lightw. Technol. 34 (14) (2016) 3348–3353, https://doi.org/10.1109/JLT.2016.2563521.

[21] F. Chiavaioli, P. Biswas, C. Trono, S. Jana, S. Bandyopadhyay, N. Basumallick, A. Giannetti, S. Tombelli, S. Bera, A. Mallick, F. Baldini, Sol−gel-based titania−-silica thin film overlay for long period fiber grating-based biosensors, Anal. Chem. 87 (24) (2015) 12024–12031, https://doi.org/10.1021/acs.analchem.5b01841.

[22] M. Smietana, J. Szmidt, M. Dudek, P. Niedzielski, Optical properties of diamond-like cladding for optical fibres, Diam. Relat. Mater. 13 (2004) 954–957, https://doi.org/10.1016/j.diamond.2003.12.003.

[23] L. Coelho, D. Viegas, J.L. Santos, J.M. de Almeida M.M., Characterization of zinc oxide coated optical fiber long period gratings with improved refractive index sensing properties, Sensor Actuat B-Chem. 223 (2016) 45–51, https://doi.org/10.1016/j.snb.2015.09.061.

[24] J. Zhang, X. Tang, J. Dong, T. Wei, H. Xiao, Zeolite thin film-coated long period Fiber grating sensor for measuring trace chemical, Opt. Express 16 (11) (2008) 8317–8323, https://doi.org/10.1364/OE.16.008317.

[25] M. Smietana, M. Koba, E. Brzozowska, K. Krogulski, J. Nakonieczny, L. Wachnicki, P. Mikulic, M. Godlewski, W.J. Bock, Label-free sensitivity of long-period gratings enhanced by atomic layer deposited TiO2 nano-overlays, Opt. Express 23 (7) (2015) 8441–8453, https://doi.org/10.1364/OE.23.008441.

[26] S. Bandyopadhyay, N. Basumallick, S. Bysakh, T. Dey, P. Biswas, S. Bandyopadhyay, Design of turn around point long period fiber grating sensor with Au-nanoparticle self monolayer, Opt. Laser Technol. 102 (2018) 254–261, https://doi.org/10.1016/j.optlastec.2017.12.025.

[27] M. Smietana, M. Koba, P. Mikulic, W.J. Bock, Towards refractive index sensitivity of long period gratings at level of tens of μm per refractive index unit: fiber cladding etching and nano-coating deposition, Opt. Express 24 (11) (2016) 11897–11904, https://doi.org/10.1364/OE.24.011897.

[28] S. Bandyopadhyay, I. Del Villar, N. Basumallick, P. Biswas, T. Dey, S. Bandyopadhyay, Long period fiber grating for biosensing: an improved design methodology to enhance add-layer sensitivity, IEEE J. Lightw. Technol. 36 (4) (2018) 1178–1184, https://doi.org/10.1109/JLT.2017.2754549.

[29] M. Piestrzynska, M. Dominik, K. Kosielb, M.J. Katarzyna, S. Karpinska, E. Brzozowska, L. Shao, J. Jonsson, W.J. Bock, M. Smietana, Ultrasensitive tantalum oxide nano-coated long period gratings for detection of various biological targets, Biosens. Bioelectron. 133 (2019) 8–15, https://doi.org/10.1016/j.bios.2019.03.006.

[30] F. Esposito, A. Zotti, R. Ranjan, S. Zuppolini, A. Borriello, S. Campopiano, A. Iadicicco, Single-ended long period Fiber grating coated with polystyrene thin film for butane gas sensing, IEEE J. Lightw. Technol. 36 (2018) 825–832, https://doi.org/10.1109/JLT.2017.2776599.

[31] J. Hromadka, B. Tokay, R. Correia, S.P. Morgan, S. Korposh, Highly sensitive volatile organic compounds vapour measurement susing a long period grating optical fibre sensor coated with metalorganic framework ZIF-8, Sensor Actuat B-Chem 260 (2018) 685–692, https://doi.org/10.1016/j.snb.2018.01.015.

[32] J. Hromadka, B. Tokay, R. Correia, S.P. Morgan, S. Korposh, Carbon dioxide measurements using long period grating optical fibre sensor coated with metal organic framework HKUST-1, Sensor Actuat B-Chem 255 (2018) 2483–2494, https://doi.org/10.1016/j.snb.2017.09.041.

[33] F. Esposito, L. Sansone, C. Taddei, S. Campopiano, M. Giordanob, A. Iadicicco, Ultrasensitive biosensor based on long period grating coated with polycarbonate-graphene oxide multilayer, Sensor Actuat B-Chem 274 (2018) 517–526, https://doi.org/10.1016/j.snb.2018.08.002.

[34] S. Bandyopadhyay, P. Biswas, F. Chiavaioli, C. Trono, N. Basumallick, F. Baldini, S. Bandyopadhyay, Long-period fiber grating: a specific design for biosensing applications, Appl 56 (2017) 9846–9853, https://doi.org/10.1364/AO.56.009846.

[35] L Wang, W Zhang, B Wang, L Chen, Z Bai S Gao, J Li, Y Liu, "Simultaneous strain and temperature measurement by cascading few-mode fiber and single-mode fiber long-period fiber gratings" Appl. 53, 2013, 7045–7049, DOI: https://doi.org/10.1364/AO.53.007045.

[36] J. Sang, Z. Gu, Q. Ling, W. Feng, Film sensor based on cascaded tilted long-period and tilted fiber Bragg grating, J. Opt. 20 (2018) 065402–065406.

[37] E. Anemogiannis, E.N. Glytsis, T.K. Gaylord, Transmission characteristics of long-period fiber gratings having arbitrar azimuthal/radial refractive index variations, IEEE J. Lightw. Technol. 21 (1) (2003) 218–227, https://doi.org/10.1109/JLT.2003.808637.

[38] Y. Koyamada, Numerical analysis of core-mode to radiation-mode coupling in long-period fiber gratings, IEEE Photonic Tech L. 13 (4) (2001) 308–310, https://doi.org/10.1109/68.917834.

[39] T. Erdogan, Cladding-mode resonances in short- and long period fiber grating filters, J. Opt. Soc. Am. A 14 (8) (1997) 1760–1763, https://doi.org/10.1364/JOSAA.14.001760.

[40] T. Erdogan, Fiber grating spectra, IEEE J. Lightw. Technol. 15 (8) (1997) 1277–1294, https://doi.org/10.1109/50.618322.

[41] N.J. Geddes, A.S. Martin, F. Caruso, R.S. Urquhart, D.N. Furlong, J.R. Sambles, K.A. Than, J.A. Edger, Immobilisation of IgG onto gold surfaces and its interaction with anti-IgG studied by surface plasmon resonance, J. Immunol. Methods 175 (2) (1994) 149–169, https://doi.org/10.1016/0022-1759(94)90358-1.

[42] K. Saha, S.S. Agasti, C. Kim, X. Li, V.M. Rotello, Gold nanoparticles in chemical and biological sensing, Chem. Rev. 112 (5) (2012) 2739–2779, https://doi.org/10.1021/cr2001178.

[43] N. Basumallick, P. Biswas, R. Mark Carter, R.R.J. Maier, S. Bandyopadhyay, K. Dasgupta, S. Bandyopadhyay, Design of palladium-coated long-period fiber grating for hydrogen sensing, IEEE J. Lightw. Technol. 34 (21) (2016) 4912–4919, https://doi.org/10.1109/JLT.2016.2604481.

[44] C. Zhou, J.-M. Friedt, A. Angelova, K.-H. Choi, W. Laureyn, F. Frederix, L.A. Francis, A. Campitelli, Y. Engelborghs, G. Borghs, Human immunoglobulin adsorption investigated by means of quartz crystal microbalance dissipation, atomic force microscopy, surface acoustic wave, and surface Plasmon resonance techniques, Langmuir 20 (14) (2004) 5870–5878, https://doi.org/10.1021/la036251d.

[45] J.P. Busalmen, S.R. De sanchez, D.J. Schiffrin, Ellipsometric measurement of bacterial films at metal-electrolyte interfaces, Appl. Environ. Microbiol. 64 (10) (1998) 3690–3697.

[46] C. Walthman, J. Boyle, B. Ramey, J. Smit, Light scattering and adsorption caused by bacterial activity in water, Appl. 33 (31) (1994), https://doi.org/10.1364/AO.33.007536 7536–7340.

[47] B.E. Burdge, S. Nr, The measurement of mass thickness and density in the electron microscope, J. Biophys. Biochem. Cytol. 8 (1) (1960) 1–11, https://doi.org/10.1083/jcb.8.1.1.

[48] G. Ligay, F.E. Meunier-Prest, C. Malki, N. Latruffe, A. Dereux, DNA Nanofilm thickness measurement on microarray in air and in liquid using an atomic force microscope, Biosens. Bioelectron. 21 (4) (2005) 627–636, https://doi.org/10.1016/j.bios.2004.12.021.

[49] M. Kinnunen, A. Kauppila, A. Karmenyan, R. Myllyla, Effect of the size and shape of a red blood cell on elastic light scattering properties at the single-cell level, Biomed. Opt. Express 2 (7) (2011) 1802–1814, https://doi.org/10.1364/BOE.2.001803.

[50] L. Marques, F.U. Hernandez, S.W. James, S.P. Morgan, M. Clark, R.P. Tatam, S. Korposh, Highly sensitive optical fibre long period grating biosensor anchored with silica core gold shell nanoparticles, Biosens. Bioelectron. 75 (2016) 222–231, https://doi.org/10.1016/j.bios.2015.08.046.

[51] N. Elahi, M. Kamali, M. Hadi Baghersad, Recent biomedical applications of gold nanoparticles: a review, Talanta 184 (2018) 537–556, https://doi.org/10.1016/j.talanta.2018.02.088.

[52] M. Smietana, W.J. Bock, J. Szmidt, G.R. Pickwell, Advances in material science for environment and nuclear technology, in: Kevin Fox Elizabeth Hoffman Navin Manjooran Gary Pickrell (Ed.), Advances in Materials Science for Environmental and Nuclear Technology, American Ceramic Society, Pittsburgh, 2010, pp. 275–286.

[53] Peter M. Martin, Handbooks of Deposition Techniques of Thin Films and Coatings, 3rd ed., Elsevier. Inc, 2010.